Journal of Hazardous Materials 276 (2014) 262–270

Contents lists available at ScienceDirect

Journal of Hazardous Materials

journal homepage: www.elsevier.com/locate/jhazmat

Rapid and selective detection of acetone using hierarchical ZnO gas sensor for hazardous odor markers application

Qianqian Jia, Huiming Ji*, Ying Zhang, Yalu Chen, Xiaohong Sun**, Zhengguo Jin

Key Laboratory of Advanced Ceramics and Machining Technology of Ministry of Education, School of Materials Science and Engineering, Tianjin University, Tianjin 300072, China

HIGHLIGHTS

- ZnO spheres fabricated via solvothermal method are with (0 0 2) polar facet exposed.
- Response time of ZnO sensor for detecting 100 ppm acetone is as short as 3 s.
- R_a/R_g toward 100 ppm acetone is 33 when operated at 230 °C.
- ZnO sensor exhibits good selectivity against other toxic gases and water vapor.
- Porous structure and exposure of polar facet contribute to good sensing properties.

ARTICLE INFO

Article history:
Received 5 February 2014
Received in revised form 16 April 2014
Accepted 14 May 2014
Available online 22 May 2014

Keywords:
ZnO
Hierarchical nanostructure
Rapid
Selective
Acetone sensor

ABSTRACT

Hierarchical nanostructured ZnO dandelion-like spheres were synthesized via solvothermal reaction at 200 °C for 4 h. The products were pure hexagonal ZnO with large exposure of (0 0 2) polar facet. Side-heating gas sensor based on hierarchical ZnO spheres was prepared to evaluate the acetone gas sensing properties. The detection limit to acetone for the ZnO sensor is 0.25 ppm. The response (R_a/R_g) toward 100 ppm acetone was 33 operated at 230 °C and the response time was as short as 3 s. The sensor exhibited remarkable acetone selectivity with negligible response toward other hazardous gases and water vapor. The high proportion of electron depletion region and oxygen vacancies contributed to high gas response sensitivity. The hollow and porous structure of dandelion-like ZnO spheres facilitated the diffusion of gas molecules, leading to a rapid response speed. The largely exposed (0 0 2) polar facets could adsorb acetone gas molecules easily and efficiently, resulting in a rapid response speed and good selectivity of hierarchical ZnO spheres gas sensor at low operating temperature.

1. Introduction

With the rapid development of industry, the volatilization of hazardous gases such as acetone, ammonia, and toluene has become a serious problem which is harmful to human health and safety [1]. Particularly, acetone, which is widely used as good solvent and raw material for organic synthesis, can volatilize easily and cause damages to eyes, noses, and central nervous system when the concentration is higher than 450 mg/m^3 (173 ppm). Besides, acetone in human breath is a biomarker for type-1 diabetes [2]. The acetone concentration from the breath of healthy body is lower than 0.8 ppm, while that from a diabetic patient is higher than 1.8 ppm [3,4]. Therefore, the development of gas sensors for rapid and selective detection of acetone attracts the interest of researchers in recent years.

Among several gas sensing materials studied so far, zinc oxide (ZnO) is a wide-band-gap semiconducting material (E_g = 3.37 eV) with good sensing properties toward various oxidizing and reducing gases. It has the advantages of low cost, simplicity in fabrication, and miniaturized [5–7]. Compared with bulk materials, nanostructured ZnO exhibit more excellent gas sensing properties [8–10]. Specially, hierarchical nanostructures using lower dimension nanocrystals as the building blocks attract more interest due to their less gas diffusion length, higher mobility, and relatively larger specific surface area than the agglomerated nanoparticles [11]. Up to now, hierarchical ZnO architectures with different shapes were synthetized by chemical vapor deposition [12], thermal oxidation method [13], microwave hydrothermal [14], and solvothermal method [15], and they were used as gas sensing

* Corresponding author. Tel.: +86 022 27890485.
** Corresponding author. Tel.: +86 022 27406114.
E-mail addresses: jihuiming@tju.edu.cn (H. Ji), sunxh@tju.edu.cn (X. Sun).

http://dx.doi.org/10.1016/j.jhazmat.2014.05.044
0304-3894/

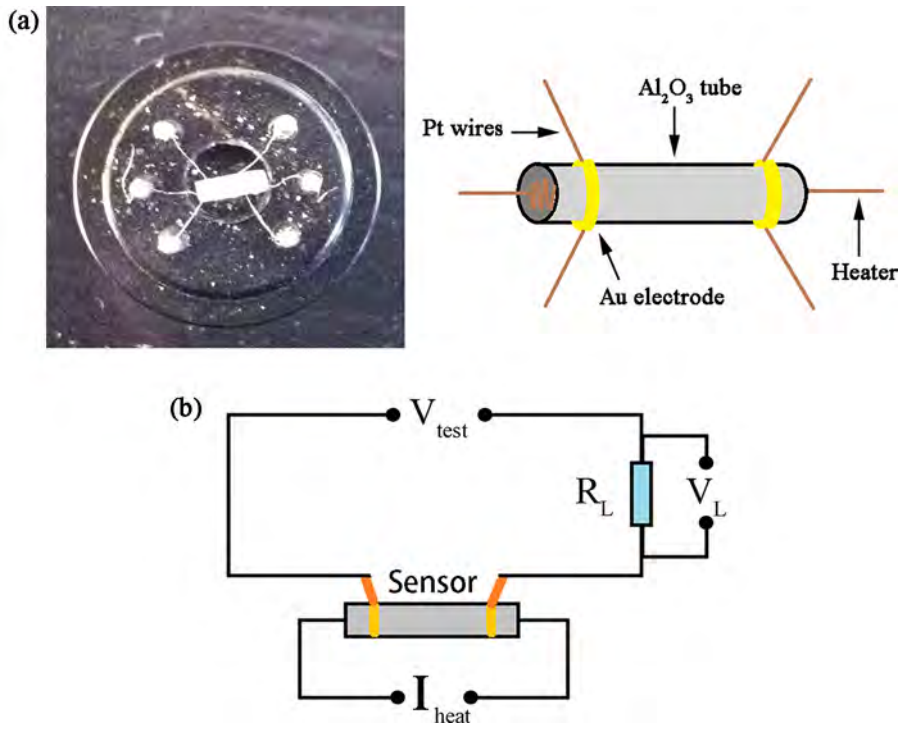

Fig. 1. (a) Digital photo and schematic diagram of a typical gas sensor and (b) measuring electric circuit of gas sensing properties.

materials. Urchin-like ZnO spheres exhibited excellent selectivity and fast response to acetone; however, the response to 100 ppm acetone was not very high ($R_a/R_g = 10$) [16]. The response of porous ZnO nanostructures and nest-like 3D ZnO hierarchically structures to 100 ppm acetone were 20.27 and 17.4, respectively, but the operating temperature was too high (400 and 420 °C) [17,18]. The response of ZnO hollow nanofibers to 100 ppm acetone was 67.7 operated at 220 °C, which was one of the highest response reported so far [19]. Nevertheless, the response time (17 s) was slightly longer [20,21] due to the limited rate of the adsorption–desorption on the fiber surface at 220 °C [22]. Since there are a lot of problems exist in the acetone detection research, acetone gas sensors with high sensitivity, short response time, low working temperature, and good selectivity are urgently needed.

In our previous work, the preparation conditions of dandelion-like ZnO were fully discussed and the ZnO materials exhibited gas response to ethanol [23]. In this work, we present a further study of the prepared hierarchical ZnO spheres concerning the hazardous odors (acetone particularly) sensing properties for application as the acetone gas sensor. The gas sensing mechanisms are discussed in detail.

2. Experimental

2.1. Synthesis of hierarchical ZnO spheres

The hierarchical ZnO spheres were fabricated via a simple solvothermal method. In a typical synthesis, 0.702 g $Zn(CH_3COO)_2{\cdot}2H_2O$ was dissolved in 40 mL of ethanolamine with magnetic stirring to form a homogeneous solution. The solution was transferred into a Teflon-lined stainless autoclave (50 mL capacity). The sealed autoclave was maintained at 200 °C for 4 h and 6 h, separately, and then cooled to room temperature. White precipitates were centrifuged and washed alternately with distilled water and ethanol for several times. Finally, the obtained products were dried in air at 80 °C for 4 h.

2.2. Characterization

The morphology of the synthesized ZnO was investigated by scanning electron microscope (SEM: Hitachi, S4800), transmission electron microscopy and high-resolution transmission electron microscopy (TEM, HR-TEM, FEI Tecnai G2 F20). The crystalline structures were examined by X-ray diffraction (XRD) via a Rigaku D/max 2500 diffractometer at 40 kV and 200 mA with Cu Kα radiation (λ = 0.15406 nm), ranging from 20° to 80°. The photoluminescence (PL) spectroscopy was performed at room temperature using a spectrometer (Jobin Yvon Fluorolog 3-21, Jobin Yvon Inc.) with an excitation wavelength of 325 nm. The average crystal size was calculated by Scherrer equation:

$$D = \frac{k\lambda}{B\cos\theta} \quad (1)$$

where D is the crystal size perpendicular to the facet direction, k is the Scherrer constant, λ is the wavelength of X ray (0.15406 nm), B is the peak width at half weight, and θ is the diffraction angle.

2.3. Preparation of gas sensor and measurement of gas sensing properties

Fig. 1 displays (a) the digital photo and schematic diagram of the sensor, (b) the measuring electric circuit of gas sensing properties. The preparation and measurement of the side-heating sensor were similar to those depicted in our previous report [24]. A proper amount of ZnO powder was mixed with several drops of distilled water to form a paste, which was then coated onto the alumina tube posited with a pair of Au electrodes and four Pt wires. A Ni–Cr alloy filament which was inserted into the tube was used as heater, and the temperature of coated tube was controlled by regulating the heating current. A heating current (I_{heat}) range from 0 to 300 mA was applied, and a test voltage (V_{test}) was supplied to the sensor. A load resistor R_L was connected to the sensor, whose resistance was measured and used for calculating and outputting the sensor resistance. The gas sensing properties were measured by CGS-8

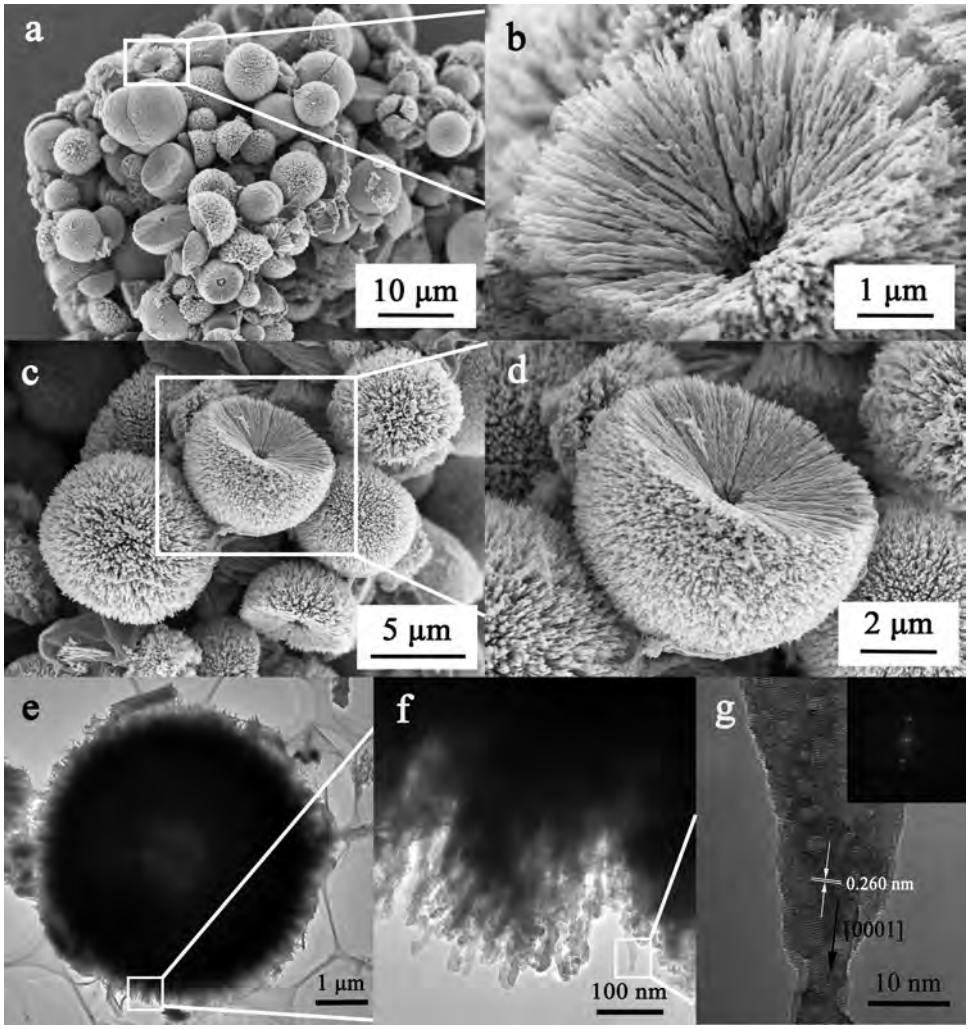

Fig. 2. (a–d) SEM images; (e, f) TEM and (g) HRTEM images (the inset FFT image) of hierarchical ZnO spheres prepared at 200 °C for 4 h.

intelligent gas sensing analysis system (Beijing Elite Tech Co. Ltd., China) with a gas tanker of 20 L. The gas sensor was aged fully for several hours at the working temperature (230 °C) before measurement to improve the mechanical strength and electrical contact, and to ensure its stability and repeatability. The sensor response (S_R) to gas is defined as

$$S_R = \frac{R_a}{R_g} \tag{2}$$

where R_a and R_g are the sensor resistance in air and in a target gas, respectively. The cross sensitivity (*CS*) to relative humidity of sensor is defined as

$$CS = abs\left[\frac{S_{25\%} - S_{RH}}{S_{25\%}}\right] \times 100\% \tag{3}$$

where S_{RH} and $S_{25\%}$ are the response sensitivity of sensor at a given relative humidity (RH) and RH = 25% defined in Eq. (2), respectively. The times to reach 90% variation in the resistance upon different gases are defined as the response time and recovery time, respectively.

3. Results and discussion

3.1. Material characteristics

The morphology and structure of ZnO sample reacted at 200 °C for 4 h were characterized with SEM, TEM, and HRTEM and shown in Fig. 2. As can be seen from Fig. 2(a) and (c), ZnO exhibits dandelion-like spheres with diameter range of 3–8 μm. High magnification SEM images in Fig. 2(b) and (d) indicate the dandelion-like ZnO spheres are self-assembled by numerous nanorods, whose diameter are about 10–30 nm, and composed of holes in the center part. TEM image of a single ZnO sphere in Fig. 2(e) displays a light black color in the center, further confirming its hollow structure. High magnification of TEM images in Fig. 2(f) demonstrates the characteristic of saw-tooth like brims, revealing the nanorods are orderly arranged. Fig. 2(g) is a lattice-resolved HRTEM image taken from a single ZnO nanorod. FFT image in the inset of Fig. 2(g) depicts the well-defined single crystal of ZnO nanorod. The lattice fringes are about 0.260 nm corresponding to the (0 0 2) facet of ZnO, revealing that the nanorod preferentially grows along [0 0 0 1] direction.

The XRD patterns of hierarchical ZnO spheres prepared at 200 °C for (a) 4 h and (b) 6 h are shown in Fig. 3. All typical diffraction peaks were well indexed to the profile of hexagonal ZnO (JCPDS card no. 36-1451). No impurities could be observed in the patterns. The diffraction peak width of ZnO spheres reacted for 4 h are much wider than those for 6 h, indicating fine crystals are obtained when

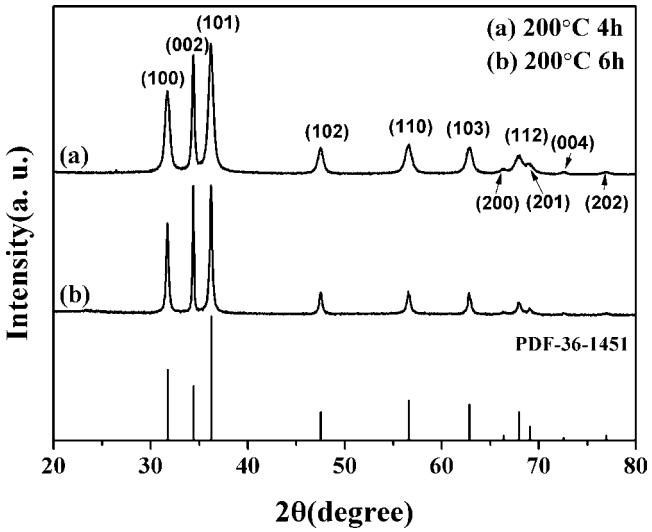

Fig. 3. XRD patterns of hierarchical ZnO spheres reacted for (a) 4 h, (b) 6 h, and profile of hexagonal ZnO (JCPDS card no. 36-1451).

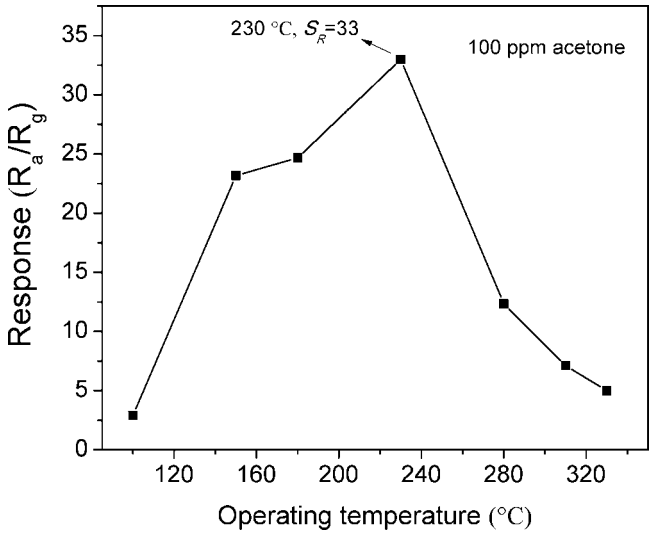

Fig. 5. Responses of ZnO spheres sensor toward 100 ppm acetone as a function of operating temperature.

the reaction time is 4 h. The diffraction intensity ratio of (0 0 2) polar facets to (1 0 0) nonpolar facets (I(0 0 2)/I(1 0 0) = 1.39) of hierarchical ZnO spheres reacted for 4 h is higher than the ZnO standard pattern (I(0 0 2)/I(1 0 0) = 0.77), indicating a large fraction exposure of polar facets [25].

The formation process of hierarchical ZnO spheres is proposed as three stages shown in Fig. 4. In this experiment, ethanolamine (EA), as the solution, plays a crucial role of complexing, assembling, and structure-directing agent in the present synthetic system. In the initial stage, the Zn source was primarily in the form of $[Zn(EA)_m]^{2+}$, where m is a positive integer. In the solvothermal process, $[Zn(EA)_m]^{2+}$ decomposed into Zn^{2+} ions and then $Zn(OH)_2$ precipitation was generated, which was decomposed into ZnO crystal nuclei at the elevating temperature as shown in Eqs. (4)–(6). This decomposition process is slow because EA is excess and prevents the nucleation density of ZnO from too high. In the second stage, the linear EA molecules adsorbed on the (0 1 0) and (1 0 0) facets of ZnO, which are in favor of anisotropic growth of the ZnO nuclei as directing agent [26]. At the same time, high energy (0 0 2) facets grow and ZnO nanorods with [0 0 0 1] orientation are obtained subsequently. These nanorods are aligned perpendicularly to the core via an "oriented attachment" process and dandelion-like spheres are generated [27]. In the third stage, the small nanoclusters and nanoparticles in the center gradually disappear and the hollow structures are eventually generated, as explained by "Ostwald ripening" mechanism [28].

$$[Zn(EA)_m]^{2+} \rightarrow Zn^{2+} + mEA \quad (4)$$

$$Zn^{2+} + 2OH^- \rightarrow Zn(OH)_2 \quad (5)$$

$$Zn(OH)_2 \rightarrow ZnO + H_2O \quad (6)$$

3.2. Gas sensing properties

Fig. 5 shows the response of ZnO spheres sensor toward 100 ppm acetone as a function of operating temperature. It is depicted that the response increases when the operating temperature varies from 100 to 230 °C, and then decreases. The maximum response reaches 33 at an optimum operating temperature of 230 °C, which is relatively lower comparing with other reports [17,18,29,30]. The sensor response varies with the operating temperature due to the surface adsorption behavior of semiconductor materials. The change of operating temperature alters the kinetics of the adsorption and the chemical reactions on the surface, leading to different sensor responses [31]. When the temperature is lower than 230 °C, the gas adsorption and surface chemical reaction dominate and the thermal energy is essential for the electrons to overcome the activation

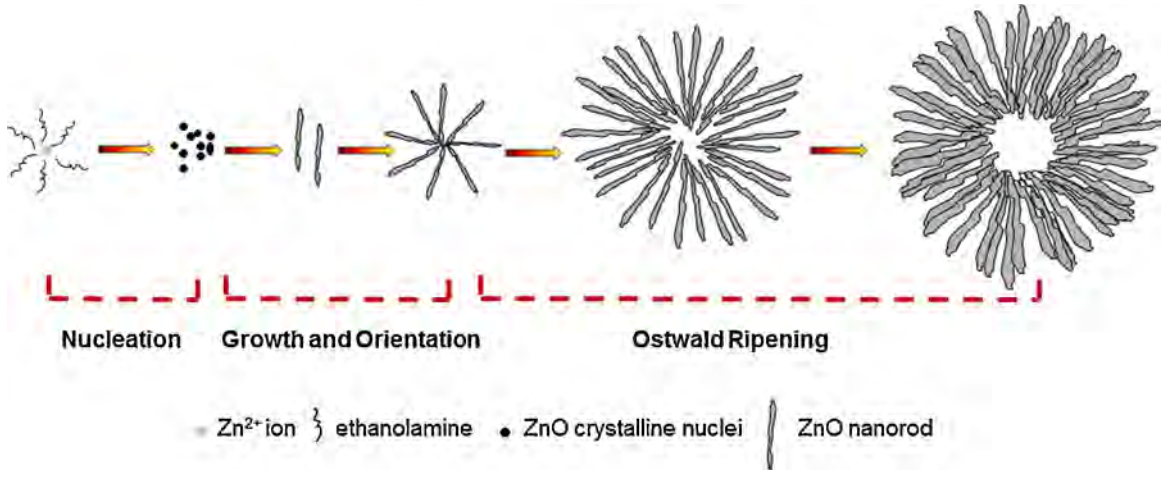

Fig. 4. Schematic diagram for the formation process of hierarchical ZnO spheres.

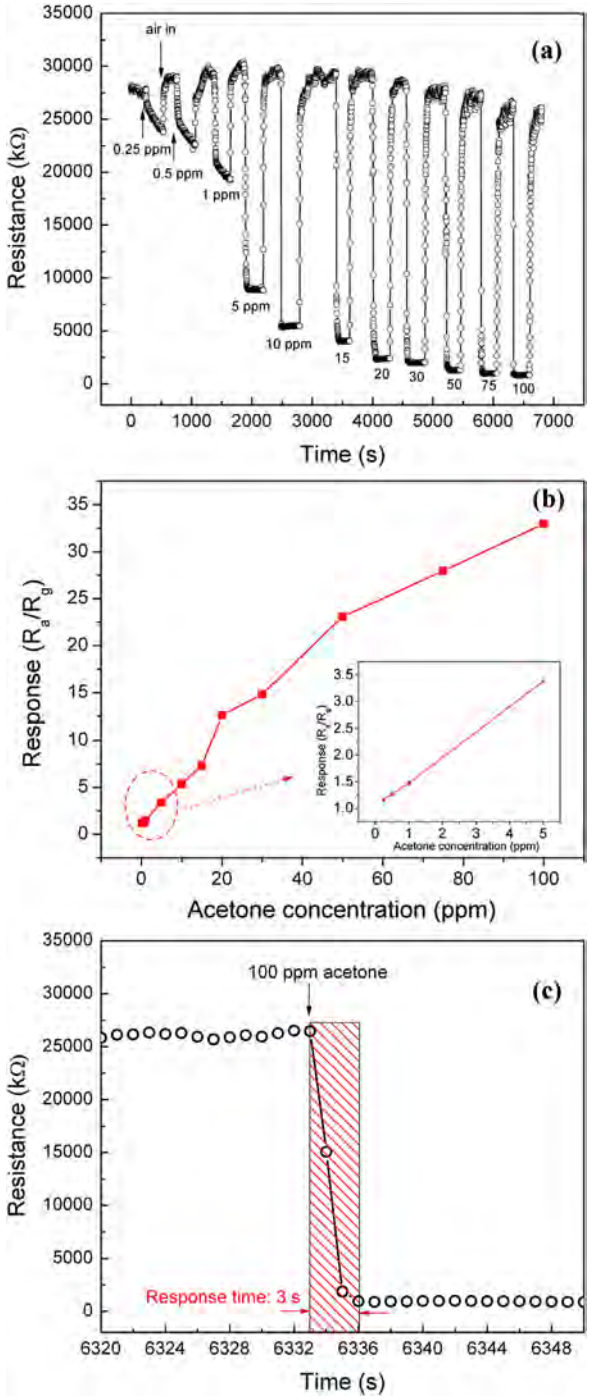

Fig. 6. (a) Sensing transient curve of ZnO spheres sensor to different concentration of acetone, (b) sensor response, and (c) response time calculated from the resistance-time data of ZnO spheres sensor to 100 ppm acetone measured at 230 °C.

energy barrier. So the response increases as the increasing of operating temperature. However, when the temperature is higher than 230 °C, desorption of gas molecules become dominant [32], which is restricted by high temperature. Thus, the response decreases at the temperature higher than 230 °C. The balances between the gas adsorption, chemical reaction, and desorption process contribute to the optimum operating temperature of ZnO spheres sensor.

The responses of the ZnO spheres sensor toward acetone in the concentration range between 0.25 and 100 ppm were measured at 230 °C and the sensing transient curve is shown in Fig. 6(a). It is noticed the detection limit to acetone for the ZnO sensor is

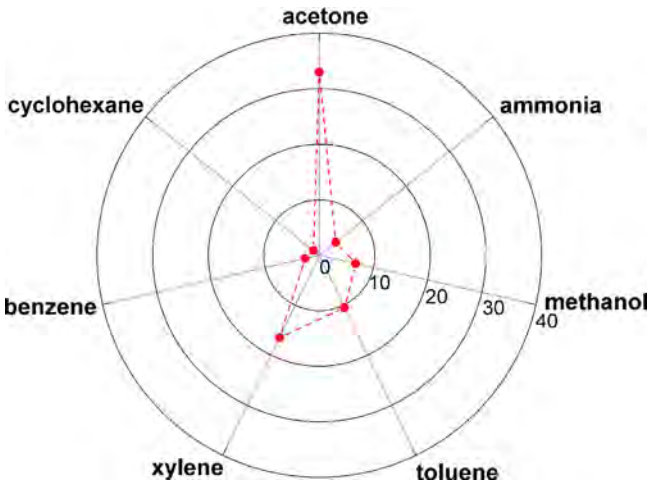

Fig. 7. Polar plot of ZnO spheres sensor responses to 100 ppm of different reducing toxic gases operated at 230 °C.

0.25 ppm, showing a response of 1.16. Fig. 6(b) displays the sensor responses toward different concentration of acetone calculated from the resistance-time data. The response increases almost linearly from 1.16 to 3.38 with the increase of acetone concentration range from 0.25 to 5 ppm, indicating the ZnO sensor has advantage in detecting low concentration of acetone and can allow precise diagnosis of diabetes by breath analysis. When exposed to 100 ppm acetone, the sensor exhibits the response of 33, showing a high level of sensing performance toward hazardous acetone gas in the environment. The response speed is also an important indicator for acetone gas detection. As calculated and depicted in Fig. 6(c), the response time of ZnO sensor toward 100 ppm acetone is 3 s, which is one of the most rapid respond as reported so far. Table 1 lists the operating temperature, response sensitivity, and response time to 100 ppm acetone in the present study and those reported in the literatures. It is observed that the sensor based on hierarchical ZnO spheres exhibits a correspondingly low working temperature, high response, and rapid response speed. The excellent acetone gas sensing performances of hierarchical ZnO spheres sensor make it a promising candidate for application in environmental detection of hazardous odors and human breath disease diagnosis.

Selectivity of the gas sensor is crucial for practical application. The responses of ZnO spheres sensor toward 100 ppm different toxic reducing gases (including acetone, NH_3, methanol, toluene, xylene, benzene, and cyclohexane) were tested at 230 °C and shown as polar plot in Fig. 7. The response to 100 ppm acetone was 2-fold and 30-fold higher than those to xylene and cyclohexane, respectively, because acetone could be easily catalyzed on the surface of the sensor [33]. This result demonstrates that the sensor is effective for detecting the highly toxic acetone gas and satisfies the requirement for actual application in environmental monitoring.

The relative humidity (RH) varies in the range of 20–60% in the ambient and 89–97% in the human breath [38]. The RH condition of our testing environment was 25%. In order to characterize the stability of sensor in the high RH air, we measured the sensor resistance as a function of RH from 25% to 40%, 60%, 80%, and 90%, and the sensor responses to different RH from 40% to 60%, 80%, and 90% (corresponding to water vapor concentration of 0.94, 1.40, 1.88, and 2.10×10^4 ppm) as shown in Fig. 8(a). The sensor resistance decreases steeply from 25.5 to 19.6 MΩ with increasing RH from 25% to 90% due to the adsorption of water-related species (e.g. OH). The reducing water-related species on the sensor surface react with the adsorbed oxygen ions, acting as the donor, and increase the sensor conductivity as a result [39]. After water vapor is injected to the gas tank, the sensor response varies from 1.15 to

Table 1
Gas response properties to 100 ppm acetone in the present study and those reported in the literatures.

ZnO sensing materials	Operating temperature (°C)	Response (R_a/R_g)	Response time (s)	Reference
Dandelion-like sphere	230	33	3	Present study
Hierarchical microsphere	320	10	1	[16]
Porous structure	400	20.27	6	[17]
Nest-like structure	420	17.4	5	[18]
Hollow nanofiber	220	67.7	17	[19]
Nanorod array	300	30.4	5	[20]
Flake	485	22.2	–	[29]
Nanotube	500	3.5	–	[30]
Flower-like structure	320	16.8	–	[34]
Hollow sphere	300	4.5	10	[35]
Mesoporous architecture	420	10.5	4	[36]
Nanosheet	340	70	9	[37]

Table 2
Response (S_R) and cross sensitivity (CS) against relative humidity of ZnO spheres sensor toward different concentration of acetone.

Acetone concentration (ppm)	25%	40%		60%		80%		90%	
	S_R	S_R	CS	S_R	CS	S_R	CS	S_R	CS
0.25	1.34	1.31	2.2%	1.25	6.7%	1.21	9.7%	1.11	17.2%
1	1.48	1.30	12.2%	1.30	12.2%	1.21	18.2%	1.21	18.2%
10	5.37	4.78	11.0%	4.48	16.6%	4.2	21.8%	4.11	23.5%

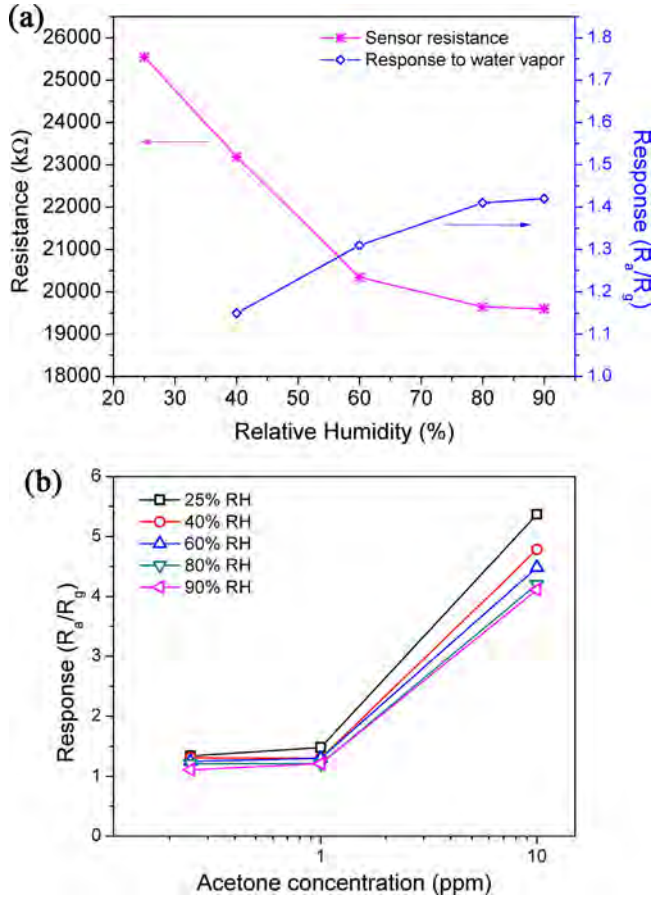

Fig. 8. (a) Sensor resistance at different RH and responses toward different concentration of water vapor and (b) sensor responses as a function of acetone concentration at different RH.

1.42 with RH increasing from 40% to 90%. It is observed that the response to 90% RH (1.42) is nearly equal to 1 ppm acetone (1.48), revealing that the sensor cannot distinguish 90% RH of water vapor from extremely low concentration of acetone (≤1 ppm). Therefore, a kind of pretreatment is needed when the sensor is used to diagnose disease from human breath. The responses of ZnO spheres sensor toward 0.25, 1, and 10 ppm acetone at the RH of 25%, 40%, 60%, 80%, and 90% separately are shown in Fig. 8(b). The response to acetone decreases with the increase of RH, exhibiting a cross sensitivity, due to the adsorbed water-related species [40]. The response (S_R) and cross sensitivity (CS) of ZnO spheres sensor toward 0.25, 1, and 10 ppm acetone are calculated by Eqs. (2) and (3) and summarized in Table 2. CS to humidity varies from ~2% to ~23%, indicating S_R is reduced by water vapor to some extent. However, S_R toward 10 ppm acetone is still larger than 4.11 at 40–90% RH, revealing the sensor exhibits good selectivity toward acetone concentration of higher than 10 ppm in the high RH environment.

3.3. Gas sensing mechanism

The gas sensing mechanism of *n*-type semiconductor oxide is based on the conductivity changes caused by adsorption and desorption of the gas molecules on the materials surface [41]. Fig. 9 shows (a) depletion region illustrations, (b) energy band gap diagrams (top) and electron density distributions (bottom) of ZnO nanorod whose section radius is "*a*". In an ideal ZnO surface without any absorption, there is no depletion region and the flat band is formed [42]. When ZnO is exposed to air, oxygen molecules adsorb on the surface and adsorbed oxygen species (O_2^-, O^-, and O^{2-}) are generated by capturing electrons from the conduction band, as represented in Eqs. (7)–(10). The regional electron depletion region is formed and the conduction band edge is bent upwards, giving rise to the donor density distribution of ZnO grain tailing as shown in the bottom of Fig. 9(b). Upon exposure to acetone, acetone molecules adsorb and donate the electrons to the pre-adsorbed oxygen species and CH^3O^-, CO_2, H_2O, etc. are formed, as shown in Eqs. (11) and (12). The electrons are returned back to ZnO, leading to the reduction of depletion region thickness and the bent degree of conduction band edge. The distribution of electron density is changed and the electron resistance reduces as a result. When the sensor is refreshed by air, the acetone molecules capture electrons and desorb from ZnO surface and thicken the depletion region, which increases the sensor resistance.

$$O_2(\text{gas}) \rightarrow O_2(\text{ads}) \quad (7)$$

$$O_2(\text{ads}) + e^- \rightarrow O_2^-(\text{ads}) \quad (8)$$

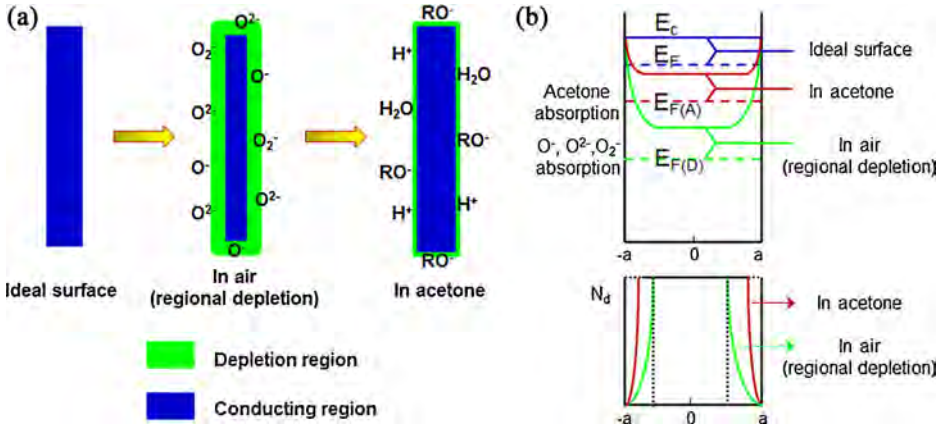

Fig. 9. (a) Depletion region illustrations, (b) energy band gap diagrams (top) and electron distributions (bottom) of acetone gas sensing of ZnO nanorod whose section radius is "*a*" (E_C: conduction band edge, E_F: Fermi level, $E_{F(D)}$: Fermi level after regional depletion, $E_{F(A)}$: Fermi level after acetone adsorption, N_d: density of electrons).

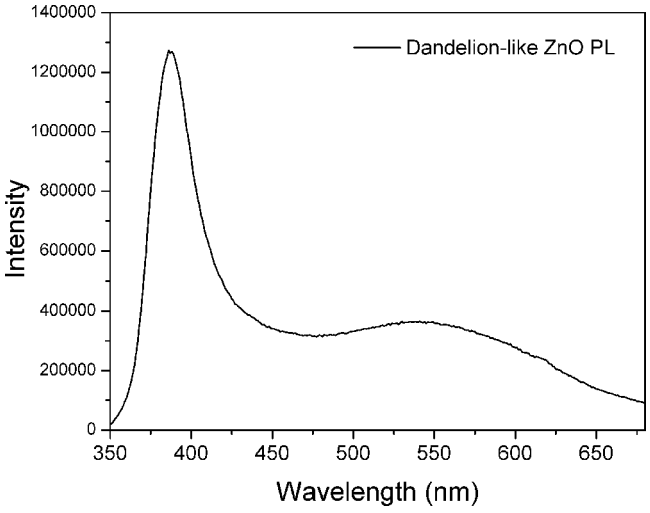

Fig. 10. Room temperature PL spectrum of hierarchical ZnO spheres.

$$O_2^-(ads) + e^- \rightarrow 2O^-(ads) \quad (9)$$

$$O^-(ads) + e^- \rightarrow O^{2-}(lat) \quad (10)$$

$$CH_3COCH_3(gas) + O^- \rightarrow CH_3COC^+H_2 + OH^- + e^- \quad (11)$$

$$CH_3COCH_3(gas) + 2O^- \rightarrow C^+H_3 + CO_2 + CH_3O^- + 2e^- \quad (12)$$

The crystal size of ZnO calculated by the Scherrer equation (1) using the fitting data of (1 0 0) peak is approximately 15 nm. The diameter (10–30 nm) and crystal size of ZnO nanorods are approaching the level of Debye length of ZnO. Therefore, when exposed to air, high proportion of volume of ZnO nanorods are depleted, and this is the first reason of high response of ZnO sensor.

The second reason is the high level of structure defects on the ZnO surface. Fig. 10 shows the room temperature PL spectrum of dandelion-like ZnO spheres. The luminescence band centered at 386 nm (3.22 eV) indicates the near-band-edge (3.37 eV) emission and free-exciton peak of ZnO [43]. The broad luminescence band around at 540 nm, which locates in the green light region (from 500 to 560 nm), is related to the oxygen vacancy detects [43–45]. This result suggests a certain amount of oxygen vacancies in dandelion-like ZnO spheres. These oxygen vacancies act as preferential adsorption sites for oxidizing gas molecules [46], so more oxygen species can be absorbed on the ZnO surface. Once ZnO is exposed in acetone, more acetone molecules can react with the absorbed oxygen species. Furthermore, more structural detects could contribute to the increase of the barrier height of electron mobility, leading to high electric resistance and gas response.

Thirdly, the superior gas sensing properties of ZnO sensor can be attributed to the exotic structural feature of dandelion-like ZnO spheres. As shown in Fig. 11(a), the porous and permeable hierarchical nanostructure allows the gas molecules diffuse rapidly throughout the hollow spheres and the sensing film, resulting in its fast gas response speed [11]. When exposed to acetone, the gas molecules contact with surface of ZnO spheres firstly, which are consisted of dominantly exposed (0 0 2) facets. The donated electrons transfer along the ZnO nanorods and across the junctions of different nanorods at the center of spheres. The transfer speed could be fast due to efficient electrons transport ways provided by

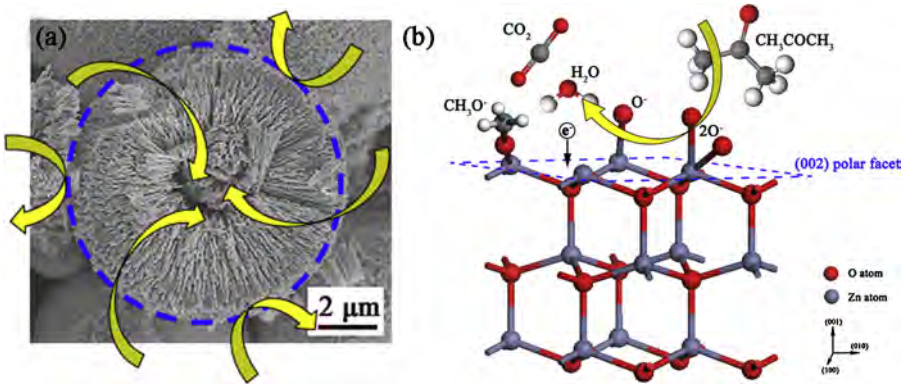

Fig. 11. Illustration of acetone sensing mechanism on (a) dandelion-like ZnO spheres and (b) (0 0 2) polar facets of hierarchical ZnO sensor.

one-dimensional ZnO nanorods [47]. Moreover, all of the Zn atoms at (0 0 2) surface of hexagonal ZnO are unsaturated coordinated, exhibiting the most dangling bonds [33]. Thus, the predominant exposed polar (0 0 2) facets are highly polarized and contain more oxygen vacancies [10,33,48]. Acetone has larger dipole moment (2.88 D) than other gases [49], which is more likely to adsorb and react with the polar (0 0 2) facets, as illustrated in Fig. 11(b), resulting in good sensing selectivity of ZnO sensor toward acetone. This unique structure constitutes a significant reason for low operating temperature, rapid and selective acetone response of sensor based on dandelion-like ZnO spheres.

4. Conclusions

Gas sensor using hierarchical ZnO spheres was fabricated and the gas sensing performance was measured. The ZnO spheres were dandelion-like with numerous nanorods with diameter range of 10–30 nm and large quantity of (0 0 2) polar facets exposed. The ZnO spheres sensor could detect acetone concentration as low as 0.25 ppm. The response of gas sensor operated at 230 °C was 33 toward 100 ppm acetone and its response time was 3 s, which was shorter than most of the reported results. The ZnO spheres sensor exhibited remarkable selectivity against several reducing hazardous gases such as NH_3, methanol, toluene, xylene, benzene, and cyclohexane. Cross sensitivity of sensor to humidity was moderate and the water vapor had no effect on the application of ZnO sensor. The small diameter and average crystal size of ZnO nanorod, plenty of oxygen vacancies, hollow and porous structural feature, and high level of exposed (0 0 2) polar facets contributed to the high response and selectivity, low working temperature, and short response time to acetone of our dandelion-like ZnO gas sensor.

Acknowledgment

The authors are grateful for financial support from the National Natural Science Foundation of China (Grant nos. 51172157 and 51202159).

References

[1] M.M. Ayad, G.E. Hefnawey, N.L. Torad, A sensor of alcohol vapours based on thin polyaniline base film and quartz crystal microbalance, J. Hazard. Mater. 168 (2009) 85–88.
[2] L. Wang, A. Teleki, S.E. Pratsinis, P.I. Gouma, Ferroelectric WO_3 nanoparticles for acetone selective detection, Chem. Mater. 20 (2008) 4794–4796.
[3] C. Deng, J. Zhang, X. Yu, W. Zhang, X. Zhang, Determination of acetone in human breath by gas chromatography–mass spectrometry and solid-phase microextraction with on-fiber derivatization, J. Chromatogr. B 810 (2004) 269–275.
[4] A.M. Diskin, P. Španěl, D. Smith, Time variation of ammonia, acetone, isoprene and ethanol in breath: a quantitative SIFT-MS study over 30 days, Physiol. Meas. 24 (2003) 107–119.
[5] X. Wu, K.W. Li, H. Wang, Facile fabrication of porous ZnO microspheres by thermal treatment of ZnS microspheres, J. Hazard. Mater. 174 (2010) 573–580.
[6] A.R. Raju, C.N.R. Rao, Gas-sensing characteristics of ZnO and copper-impregnated ZnO, Sens. Actuators B 3 (1991) 305–310.
[7] A. Jones, T.A. Jones, B. Mann, J.G. Firth, The effect of the physical form of the oxide on the conductivity changes produced by CH_4, CO and H_2O on ZnO, Sens. Actuators 5 (1984) 75–88.
[8] Q. Wu, X. Chen, P. Zhang, Y. Han, X. Chen, Y. Yan, S. Li, Amino acid-assisted synthesis of ZnO hierarchical architectures and their novel photocatalytic activities, Cryst. Growth Des. 8 (2008) 3010–3018.
[9] S. Ma, R. Li, C. Lv, W. Xu, X. Gou, Facile synthesis of ZnO nanorod arrays and hierarchical nanostructures for photocatalysis and gas sensor applications, J. Hazard. Mater. 192 (2011) 730–740.
[10] G.R. Li, T. Hu, G.L. Pan, T.Y. Yan, X.P. Gao, H.Y. Zhu, Morphology–function relationship of ZnO: polar planes, oxygen vacancies, and activity, J. Phys. Chem. C 112 (2008) 11859–11864.
[11] J.H. Lee, Gas sensors using hierarchical and hollow oxide nanostructures: overview, Sens. Actuators B 140 (2009) 319–336.
[12] Y. Li, M. Zheng, L. Ma, M. Zhong, W. Shen, Fabrication of hierarchical ZnO architectures and their superhydrophobic surfaces with strong adhesive force, Inorg. Chem. 47 (2008) 3140–3143.
[13] L.L. Wang, H.Y. Wang, Y.Q. Wang, X.J. Li, Highly sensitive and selective ethanol sensor based on micron-sized zinc oxide porous-shell hollow spheres, Mater. Res. Bull. 47 (2012) 2178–2181.
[14] Z. Jing, J. Zhan, Fabrication and gas-sensing properties of porous ZnO nanoplates, Adv. Mater. 20 (2008) 4547–4551.
[15] H. Zhang, J. Wu, C. Zhai, N. Du, X. Ma, D. Yang, From ZnO nanorods to 3D hollow microhemispheres: solvothermal synthesis, photoluminescence and gas sensor properties, Nanotechnology 18 (2007) 455604.
[16] Z. Lou, Y. Feng, X. Liu, L. Wang, T. Zhang, Acetone sensing properties of hierarchical ZnO urchinlike structures by hydrothermal process, Biomed. Eng. Appl. Basis Commun. 24 (2012) 99–103.
[17] H. Song, H. Yang, X. Ma, A comparative study of porous ZnO nanostructures synthesized from different zinc salts as gas sensor materials, J. Alloys Compd. 578 (2013) 272–278.
[18] X. Wang, W. Liu, J. Liu, F. Wang, J. Kong, S. Qiu, C. He, L. Luan, Synthesis of nestlike ZnO hierarchically porous structures and analysis of their gas sensing properties, ACS Appl. Mater. Interfaces 4 (2012) 817–825.
[19] S. Wei, M. Zhou, W. Du, Improved acetone sensing properties of ZnO hollow nanofibers by single capillary electrospinning, Sens. Actuators B 160 (2011) 753–759.
[20] Y. Zeng, T. Zhang, M. Yuan, M. Kang, G. Lu, R. Wang, H. Fan, Y. He, H. Yang, Growth and selective acetone detection based on ZnO nanorod arrays, Sens. Actuators B 143 (2009) 93–98.
[21] Q. Qi, T. Zhang, L. Liu, X. Zheng, Q. Yu, Y. Zeng, H. Yang, Selective acetone sensor based on dumbbell-like ZnO with rapid response and recovery, Sens. Actuators B 134 (2008) 166–170.
[22] A. Kolmakov, M. Moskovits, Chemical sensing and catalysis by one-dimensional metal-oxide nanostructures, Annu. Rev. Mater. Res. 34 (2004) 151–180.
[23] Y. Zhang, H. Ji, Y. Chen, X. Sun, A simple one-step solvothermal synthesis of hierarchically structured ZnO hollow spheres for enhanced selective ethanol sensing properties, J. Mater. Sci. Mater. Electron. 25 (2014) 573–580.
[24] P. Gao, H. Ji, Y. Zhou, X. Li, Selective acetone gas sensors using porous WO_3–Cr_2O_3 thin films prepared by sol–gel method, Thin Solid Films 520 (2012) 3100–3106.
[25] Y. Lu, L. Wang, D. Wang, T. Xie, L. Chen, Y. Lin, A comparative study on plate-like and flower-like ZnO nanocrystals surface photovoltage property and photocatalytic activity, Mater. Chem. Phys. 129 (2011) 281–287.
[26] S. Li, Z. Wu, W. Li, Y. Liu, R. Zhuo, D. Yan, W. Jun, P. Yan, One-pot synthesis of ZnS hollow spheres via a low-temperature, template-free hydrothermal route, Cryst. Eng. Commun. 15 (2013) 1571–1577.
[27] B. Liu, H.C. Zeng, Fabrication of ZnO dandelions via a modified Kirkendall process, J. Am. Chem. Soc. 126 (2004) 16744–16746.
[28] M. Mo, J.C. Yu, L. Zhang, S.K.A. Li, Self-assembly of ZnO nanorods and nanosheets into hollow microhemispheres and microspheres, Adv. Mater. 17 (2005) 756–760.
[29] W. Wen, J.M. We, Y.D. Wang, Large-size porous ZnO flakes with superior gas-sensing performance, Appl. Phys. Lett. 100 (2012) 262111.
[30] X. Yu, F. Song, B. Zhai, C. Zheng, Y. Wang, Electrospun ZnO nanotubes and its gas sensing applications, Physica E 52 (2013) 92–96.
[31] S. Bai, K. Zhang, R. Luo, D. Li, A. Chen, C.C. Liu, Low-temperature hydrothermal synthesis of WO_3 nanorods and their sensing properties for NO_2, J. Mater. Chem. 22 (2012) 12643–12650.
[32] S. Bai, L. Chen, P. Yang, R. Luo, A. Chen, C.C. Liu, Sn/In/Ti nanocomposite sensor for CH_4 detection, Sens. Actuators B 135 (2008) 1–6.
[33] S. Tian, F. Yang, D. Zeng, C. Xie, Solution-processed gas sensors based on ZnO nanorods array with an exposed (0 0 0 1) facet for enhanced gas-sensing properties, J. Phys. Chem. C 116 (2012) 10586–10591.
[34] C. Gu, J. Huang, Y. Wu, M. Zhai, Y. Sun, J. Liu, Preparation of porous flower-like ZnO nanostructures and their gas-sensing property, J. Alloys Compd. 509 (2011) 4499–4504.
[35] P. Song, Q. Wang, Z. Yang, Acetone sensing characteristics of ZnO hollow spheres prepared by one-pot hydrothermal reaction, Mater. Lett. 86 (2012) 168–170.
[36] G. Lu, X. Wang, J. Liu, S. Qiu, C. He, B. Li, W. Liu, One-pot synthesis and gas sensing properties of ZnO mesoporous architectures, Sens. Actuators B 184 (2013) 85–92.
[37] Y. Xiao, L. Lu, A. Zhang, Y. Zhang, L. Sun, L. Huo, F. Li, Highly enhanced acetone sensing performances of porous and single crystalline ZnO nanosheets: high percentage of exposed (1 1 0) facets working together with surface modification with Pd nanoparticles, ACS Appl. Mater. Interfaces 4 (2012) 3797–3804.
[38] M. Righettoni, A. Tricoli, S.E. Pratsinis, Si WO_3 sensors for highly selective detection of acetone for easy diagnosis of diabetes by breath analysis, Anal. Chem. 82 (2010) 3581–3587.
[39] N. Bârsan, U. Weimar, Understanding the fundamental principles of metal oxide based gas sensors; the example of CO sensing with SnO_2 sensors in the presence of humidity, J. Phys.: Condens. Matter 15 (2003) R813–R839.
[40] A. Tricoli, M. Righettoni, S.E. Pratsinis, Minimal cross-sensitivity to humidity during ethanol detection by SnO_2–TiO_2 solid solutions, Nanotechnology 20 (2009) 315502.
[41] H. Meixner, U. Lampe, Metal oxide sensors, Sens. Actuators B 33 (1996) 198–202.
[42] N. Yamazoe, K. Shimanoe, Proposal of contact potential promoted oxide semiconductor gas sensor, Sens. Actuators B 187 (2013) 162–167.

[43] M.R. Alenezi, A.S. Alshammari, K.D.G.I. Jayawardena, M.J. Beliatis, S.J. Henley, S.R.P. Silva, Role of the exposed polar facets in the performance of thermally and UV activated ZnO nanostructured gas sensors, J. Phys. Chem. C 117 (2013) 17850–17858.
[44] A.B. DjurišIć, W.C.H. Choy, V.A.L. Roy, Y.H. Leung, C.Y. Kwong, K.W. Cheah, T.K.G. Rao, W.K. Chan, H.F. Lui, C. Surya, Photoluminescence and electron paramagnetic resonance of ZnO tetrapod structures, Adv. Funct. Mater. 14 (2004) 856–864.
[45] K. Vanheusden, C.H. Seager, W.L. Warren, D.R. Tallant, J.A. Voigt, Correlation between photoluminescence and oxygen vacancies in ZnO phosphors, Appl. Phys. Lett. 68 (1996) 403–405.
[46] M.W. Ahn, K.S. Park, J.H. Heo, J.G. Park, D.W. Kim, K.J. Choi, J.H. Lee, S.H. Hong, Gas sensing properties of defect-controlled ZnO-nanowire gas sensor, Appl. Phys. Lett. 93 (2008) 263103.
[47] E. Comini, C. Baratto, G. Faglia, M. Ferroni, A. Vomiero, G. Sberveglieri, Quasi-one dimensional metal oxide semiconductors: preparation, characterization and application as chemical sensors, Prog. Mater. Sci. 54 (2009) 1–67.
[48] R. Boppella, K. Anjaneyulu, P. Basak, S.V. Manorama, Facile synthesis of face oriented ZnO crystals: tunable polar facets and shape induced enhanced photocatalytic performance, J. Phys. Chem. C 117 (2013) 4597–4605.
[49] J.A. Dean, Lange's Handbook of Chemistry, New York, 1985.